Pattern Recognition Letters 33 (2012) 1019–1026

Contents lists available at SciVerse ScienceDirect

Pattern Recognition Letters

journal homepage: www.elsevier.com/locate/patrec

A reliable iris recognition algorithm based on reverse biorthogonal wavelet transform

R. Szewczyk *, K. Grabowski, M. Napieralska, W. Sankowski, M. Zubert, A. Napieralski

Department of Microelectronics and Computer Science, Technical University of Lodz, Wolczanska Street 221/223 Building B18, 90-924 Lodz, Poland

ARTICLE INFO

Article history:
Available online 7 September 2011

Keywords:
Biometrics
Iris recognition
Signatures encoding
Signatures matching
Reverse biorthogonal wavelet transform

ABSTRACT

This article describes an iris recognition algorithm designed to analyze noisy iris biometric data. The methods forming part of the authentication process were developed and optimized by the authors using visible wavelength images of an eye taken under unconstrained conditions (at a different perspectives, illuminations, occlusion grades, etc.), mainly contained in the UBIRIS.v2 database. The whole iris authentication system was submitted by the authors to the *International Iris Recognition Contest* NICE.II, where it took eighth place, while the iris segmentation stage itself took second place in the previous contest — NICE.I.

This paper is focused on the iris feature extraction stage — the method developed by the authors to analyze noisy iris biometric data. Several techniques used for more efficient and robust analysis of such images and issues concerning the best wavelet selection are also presented in this paper.

1. Introduction

One of the open problems in biometrics that limits the applicability of iris biometrics is iris identification at-a-distance and on-the-move that must be done in unconstrained imaging conditions and using potentially large databases. To broaden the usability of iris biometrics, additional analysis techniques must be developed, taking into account the specificity of the degraded images, such as light reflections from the eye's surface, occlusions and fluctuations of perspective and illumination. Most of these factors limit availability of distinctive features needed for proper recognition. Thus, recently, significant effort has been focused on authenticating objects at-a-distance and on-the-move using the iris biometrics (Proenca and Alexandre, 2010; Matey et al., 2006). This paper describes a recognition strategy, which can be used for such purposes. The presented solution was tested within the Noisy Iris Challenge Evaluation — Part II (NICE:II) contest using the UBIRIS.v2 database (Proenca et al., 2010). In the contest, the proposed solution took eighth place.

2. Description of the proposed method

In general, the proposed strategy, presented as a flowchart in Fig. 1, is similar to a well-known scenario of the authentication process. The identification starts when an image of the eye from a person located in front of the digital camera is acquired. In the process of image acquisition, a digital representation of the biometrics T_x is obtained from a real biometrics $\mathfrak{T}_x$. The next step is iris image segmentation, which identifies the area of interest, the iris texture, and transforms it into the pseudo-polar coordinate system (Daugman, 1993). In the following step, the segmented iris image is additionally processed using blue channel removal, image conversion to monochromatic, eyelid occlusions and reflections removal, eyelashes removal and resulting iris image histogram equalization.

The extraction of distinctive features and the encoding phase is a process that allows a digital template $\widehat{T}_x$ of the biometrics to be obtained. The resulting template, which is 324 bits wide and is obtained using reverse biorthogonal 3.1 wavelet, is compared to those in a database using similarity score s to search for the pattern that best matches the template using a decision threshold t. This threshold is chosen based on the assumed security strategy — see (Bolle et al., 2004).

Each part of the algorithm is explained in detail in consecutive subsections below.

2.1. Image segmentation

The image segmentation algorithm, described in detail elsewhere (Sankowski et al., 2010; Sankowski, 2009), localizes an iris in the eye image and transforms the iris region to the pseudo-polar coordinate system (Daugman, 1993) to obtain a rectangular image of iris structure, as presented in Fig. 2. The segmentation algorithm proposed by the authors was submitted to the NICE.I contest (Proenca and Alexandre, 2010), where it took second place.

* Corresponding author.
E-mail addresses: szewczyk@dmcs.p.lodz.pl (R. Szewczyk), kgrabowski@dmcs.p.lodz.pl (K. Grabowski), mnapier@dmcs.p.lodz.pl (M. Napieralska), wsan@dmcs.p.lodz.pl (W. Sankowski), mariuszz@dmcs.p.lodz.pl (M. Zubert), napier@dmcs.p.lodz.pl (A. Napieralski).
URL: http://www.irisep.dmcs.pl (R. Szewczyk).

0167-8655/$ - see front matter © 2011 Elsevier B.V. All rights reserved.
doi:10.1016/j.patrec.2011.08.018

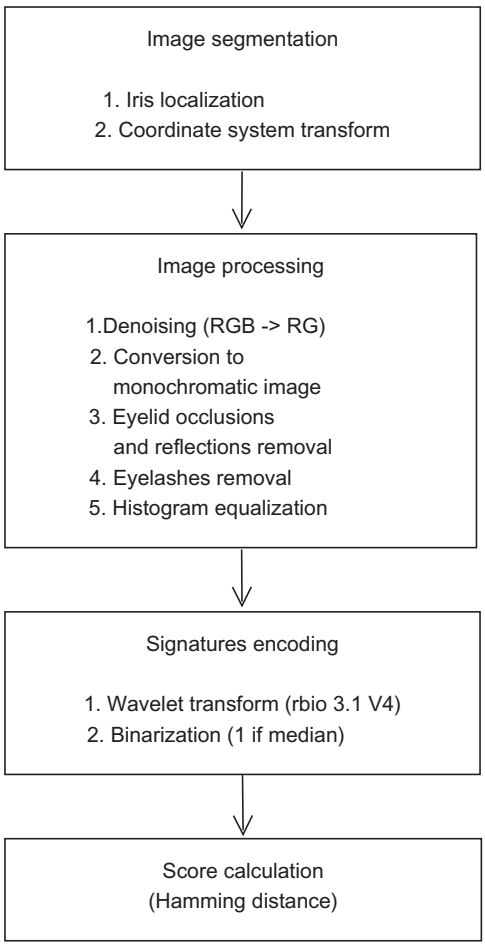

Fig. 1. The overall flowchart of the proposed method.

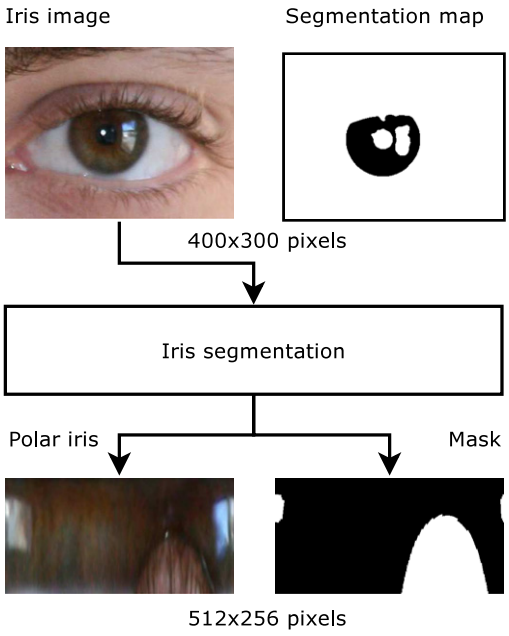

Fig. 2. Image segmentation scheme.

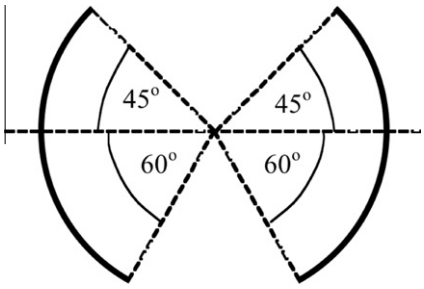

Fig. 3. Iris outer boundary search pattern (Sankowski et al., 2010).

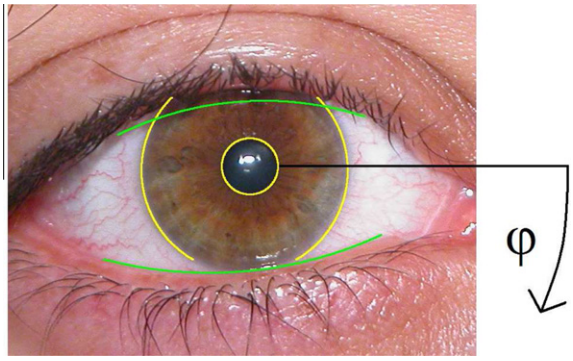

Fig. 4. Result of the iris localization process.

Iris localization consists of five sub-stages. First, the light source reflections are localized. The next stage fills in the segmented reflections in the input image. Then iris boundaries modeled as non-concentric circles are found. For the outer iris boundary, the search pattern depicted in Fig. 3 is applied. Finally, lower and upper eyelid boundaries modeled as circular arcs are localized. The result of the localization process for an eye image from the UBIRIS.v2 database (Proenca et al., 2010) is presented in Fig. 4.

After the iris localization process, the coordinate system is changed from Cartesian to the pseudo-polar one (Daugman, 1993), as depicted in Figs. 4 and 5. The transformation produces a rectangular iris structure image of size 512×256 pixels using bilinear interpolation. Additionally, the transformation generates a binary mask of the same dimensions as the rectangular iris structure image, as presented in Fig. 5. The binary mask denotes occlusions of the iris structure. White pixels in the binary mask correspond to points in the original image corresponding to reflections, eyelids and eyelashes. The authors decided to use the masks that are generated by the described segmentation algorithm rather than the ones provided by the NICE.II organizers.

2.2. Image processing

The segmented color iris image presented in Fig. 5 can be decomposed into three image components associated with the imaging wavelength spectrum: red (R), green (G) and blue (B) — $(I_{RGB} : r_{x,y}, g_{x,y}, b_{x,y} \in \{0,\ldots,255\})$. Previous research, presented in detail elsewhere (Szewczyk, 2007), showed that the blue (B) component has high amount of noise, especially for images contained in the UBIRIS database. Thus, it was decided to limit further analysis to red (R) and green (G) image components (see Fig. 6, RGB → RG). These components are transformed to the monochromatic image $I_Y(I_Y : y_{x,y} \in \{0,\ldots,255\})$ as shown in Fig. 6 (RG → grey scale image). This technique results in increasing the overall iris image Signal-to-Noise Ratio (SNR).

Afterwards, the monochromatic iris image is masked using the previously estimated noise pattern to remove eyelid occlusions and reflections that may affect the recognition process (see

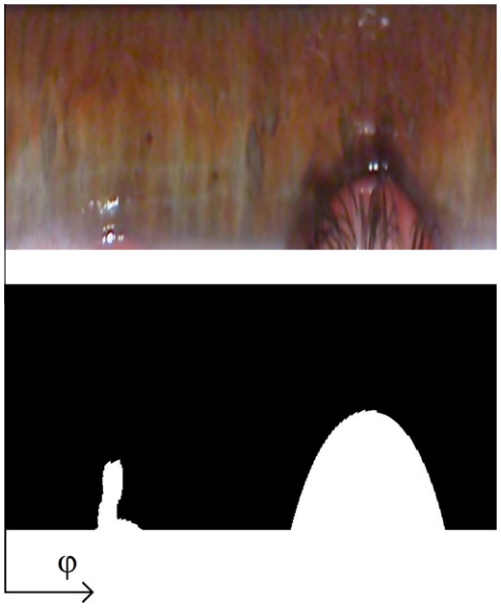

Fig. 5. The result of the coordinate system transformation: iris structure and occlusions mask in the pseudo-polar coordinate system.

Fig. 6). The noise masking can be expressed by (1) and is an operation that uses logical operation AND with image I_Y and the estimated mask M as the arguments:

$$I_{YM} = I_Y \wedge M, \tag{1}$$

where

$$I_{YM} : ym_{x,y} \in \{0,\ldots,255\},$$
$$I_Y : y_{x,y} \in \{0,\ldots,255\}, M : m_{x,y} \in \{0,1\},$$
$$x \in \{0,\ldots,511\}, y \in \{0,\ldots,255\}\}.$$

In the next step, the noise influence is additionally minimized by cropping the resulting image to half of its original size, which is then equal to 256×256 pixels. This step is one of the most important in the solution because it ensures similar amount of distinctive features in each pair of identities being compared. It can be easily shown that this part of the iris is usually not occluded by, for example, eyelids or eyelashes, while the occlusion grade of the upper part of eye can vary significantly. The cropping result is presented in Fig. 6.

Additionally, this approach decreases the computation time needed for the signature encoding stage and allows its efficient hardware implementation because most of the wavelet transforms developed for embedded systems are optimized for square images.

In the last step of the preprocessing stage, the image is normalized using a histogram equalization procedure to reduce the influence of illumination on the final recognition result (see the normalization in Fig. 6). This step is essential because the wavelet transform used in the next step for feature extraction uses amplitude rather than phase information.

2.3. An example approach to iris feature extraction

The most recognized approach for iris feature extraction is the phase-based method proposed by Daugman, which has been successfully used in the overwhelming majority of commercially available iris recognition systems. In the solution, an image of the iris is filtered by an experimentally designed filter set; details can be found elsewhere (Daugman, 1993; Daugman, 1994; Daugman, 2004; Daugman, 2007). However, many alternative

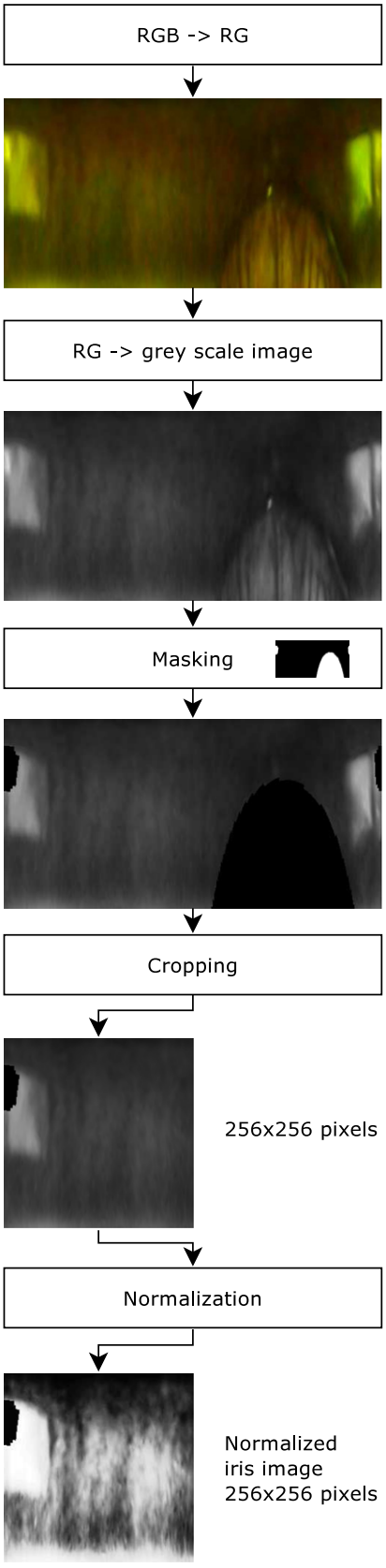

Fig. 6. The stages of image processing.

solutions have been developed for iris feature extraction. The most relevant techniques use the spatial transformation of the iris texture and correlation of templates, as suggested by Wildes (1997);

"zero-crossings wavelet representation", as proposed by Boles (1996), Boles (1997), Boles and Boashash (1998); direct wavelet packet filtering, as suggested by Noh et al. (2003); dynamic filter adjustment, as proposed by Ma et al. (2003), Ma et al. (2004); mixed wavelet approach as suggested by Kim and Ryoo (2001), Kim et al. (2004), Seong-Won (2002), Daouk et al. (2002), Ali and Hassanien (2003), Lim et al. (2001, 2004), Moukhtar et al. (2005), Poursaberi and Araabi (2005), Thornton et al. (2007), Kumar and Passi (2008), Minhas et al. (2009), Narote et al. (2009), Abhyankar and Schuckers (2009, 2010); and local binary pattern and graph matching, as proposed by Sun et al. (2005).

The main goal of this research was to develop a tool for the selection of the most distinctive features contained in an iris image. As a feature extraction method for the iris biometrics, a wavelet transform was chosen because the previous research showed that this tool is one of the most relevant for this purpose. This transform also has linear computational complexity (with respect to the size of the analyzed signal) (Strang and Nguyen, 1996) and is a very well recognized tool in the field, which additionally allows comprehensive comparison with the existing research.

As a quality measure used for selection of the best wavelet transform and for its further optimization, the tradeoff of recognition error rates is used. For this purpose, the False Acceptance Rate (FAR) and False Rejection Rate (FRR) were chosen because they are typical measures for positive biometric system efficiency, according to the Wayman's formalisms (Wayman, 1997). The tradeoff of these two rates can be expressed in several ways, which give a broad range of possibilities.

The proposed iris feature extraction method is a result of the thorough and comprehensive research on the performance of several types of wavelet transforms applied for iris recognition. In the literature, some groups of wavelets have been verified for this purpose so far. The authors decided to test as many wavelets as possible to finally choose the one that gives the best biometric efficiency, which is understood as the trade-off between False Acceptance Rate (FAR) and False Rejection Rate (FRR). The wavelets that have been verified by other researchers and the ones that have not yet been tested are grouped in separate columns in Table 1.

Using a wavelet transform, signal S can be represented in scale J by scaling coefficient $a_{J,k}$ (average component A_J) and wavelet coefficients $d_{j,k}$ (details components D_j):

$$S = \sum_k a_{J,k}\phi_{J,k} + \sum_{j=1}^{J}\sum_k d_{j,k}\Psi_{j,k} = A_J + \sum_{j=1}^{J} D_j, \tag{2}$$

where $\phi_{J,k}$ is a scaling function in scale J and shifted k times and $\Psi_{j,k}$ is a wavelet in scale j and shifted k times.

The scaling coefficient $a_{J,k}$ can be computed as follows:

$$a_{J,k} = \int f(t)\phi_{J,k}(t)dt, \tag{3}$$

while the final wavelet coefficients $d_{j,k}$ can be computed by

$$d_{j,k} = \int f(t)\Psi_{j,k}(t)dt. \tag{4}$$

The wavelet function $\Psi_{j,k}(t)$ is determined by the highpass filter with coefficients $h_1(k)$, which also produces the details of the wavelet decomposition.

$$\Psi_{j,k}(t) = \sum h_1(k)\phi_{j-1,k}(t). \tag{5}$$

The scaling function ϕ (associated with most of wavelets) is determined by the lowpass filter with coefficients $h_0(k)$ and thus it is associated with the approximations of the wavelet decomposition.

$$\phi_{j,k}(t) = \sum h_0(k)\phi_{j-1,k}(t). \tag{6}$$

Table 1
The wavelets tested, listed by wavelet families.

Family	Verified before	Newly tested
Haar	Haar	
Daubechies	db2...db11	db12...db20
Symlets	sym2...sym10	sym11...sym20
Coiflets	coif1...coif5	
Discrete Meyer		dmey
Biorthogonal	bior1.3 bior1.5	bior2.8 bior3.1
	bior2.2 bior2.4 bior2.6 bior3.3 bior3.7 bior3.9 bior5.5 bior6.8	bior3.5 bior4.4
Reverse biorthogonal		rbio1.3 rbio1.5 rbio2.2 rbio2.4 rbio2.6 rbio2.8 rbio3.1 rbio3.3 rbio3.5 rbio3.7 rbio3.9 rbio4.4 rbio5.5 rbio6.8

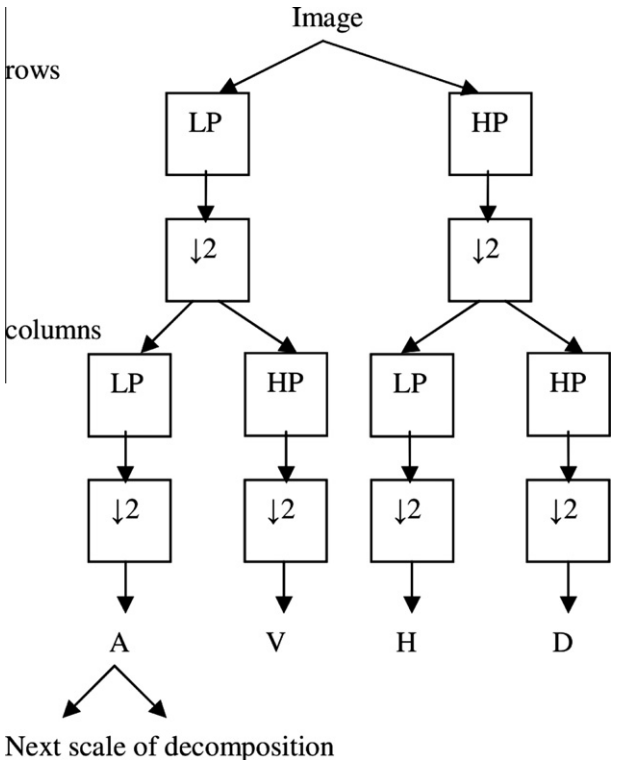

Fig. 7. The wavelet decomposition tree (LP — lowpass filter, HP — highpass filter, ↓2 — dyadic downsampling, A — approximation coefficients, V — vertical detail coefficients, H — horizontal detail coefficients, D — diagonal detail coefficients) (Szewczyk, 2007).

A wavelet transform can also be done using a diadic scale (power of two) for the wavelet scale j and wavelet shift k coefficients and is then called a Discrete Wavelet Transform (DWT). This technique allows very efficient implementation of such processing within environments where computational resource utilization must be taken into consideration. For two-dimensional signals, this transformation can be realized using the scenario presented in Fig. 7, where processing is recursively performed using typical highpass filtering (detail coefficients at the output) and lowpass filtering (approximation coefficients at the output), followed by diadic decimation for rows and columns separately.

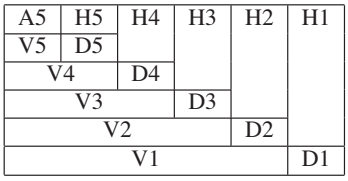

Fig. 8. The wavelet image decomposition scheme at 5th level.

Table 2
The top list of the most relevant wavelet sets obtained from 881 sets based on the EER value.

No.	EER	Wavelet	Component	Size [bits]
1	12.03%	rbio2.2	V4	400
2	12.19%	rbio3.1	V3	1156
3	13.48%	rbio3.1	V2	4356
4	14.33%	haar	V5	64
5	14.33%	rbio1.1	V5	64
6	15.68%	rbio3.1	V4	324
7	16.36%	rbio3.1	V1	16641
8	17.73%	rbio2.4	V4	576
9	19.04%	coif1	V4	400
10	19.50%	rbio2.2	V5	144
11	19.61%	bior1.3	V2	4489
12	20.04%	bior1.5	V2	4900
13	20.61%	rbio3.1	V5	100
14	20.61%	db2	V5	100
15	20.61%	sym2	V5	100
16	20.70%	haar	V3	1024
17	20.70%	rbio1.1	V3	1024
18	21.30%	haar	V4	256
19	21.30%	rbio1.1	V4	256
20	21.45%	rbio3.3	V5	196

Table 3
A statistical summary of the EER-based ranking.

Statistics	Value
Minimum	12.03%
Maximum	66.67%
Median	46.73%
Average	44.82%
Standard deviation	9.02%
Max - Min	54.65%
Max/ Min	6

Table 4
The top list of the most relevant wavelet sets obtained from 881 sets based on the d′ value.

No.	d′	Wavelet	Component	Size [bits]
1	2.2821	rbio2.2	V4	400
2	2.1764	rbio3.1	V3	1156
3	2.1185	rbio3.1	V4	324
4	2.1066	rbio3.1	V2	4356
5	1.9499	rbio1.1	V5	64
6	1.9499	haar	V5	64
7	1.9439	coif1	V4	400
8	1.8362	rbio3.1	V1	16641
9	1.8259	bior1.3	V2	4489
10	1.8117	bior1.5	V2	4900
11	1.7381	sym2	V5	100
12	1.7381	db2	V5	100
13	1.7381	rbio1.1	V3	1024
14	1.7381	haar	V3	1024
15	1.7317	rbio1.1	V2	4096
16	1.7317	haar	V2	4096
17	1.6589	bior1.5	V3	1521
18	1.5916	bior1.5	V1	17424
19	1.5735	rbio2.4	V4	576
20	1.5728	bior1.3	V3	1296

Table 5
A statistical summary of the d′-based ranking.

Statistics	Value
Maximum	2.2821
Minimum	0.0012
Median	0.2441
Average	0.3943
Standard deviation	0.4102
Max–Min	2.2809
Max/Min	1947

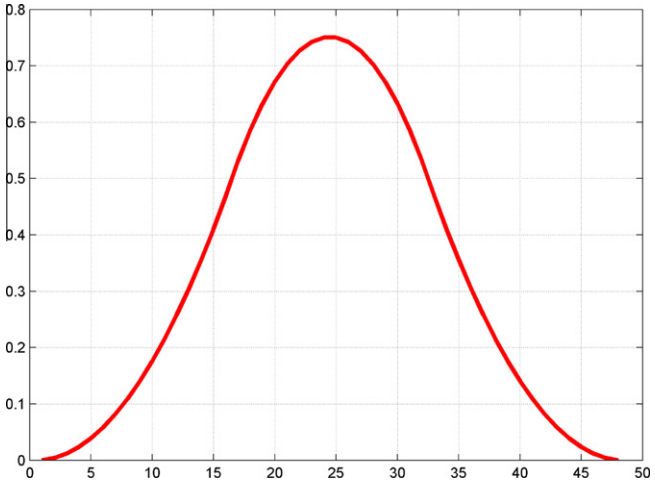

Fig. 9. The scaling function ϕ of wavelet rbio3.1.

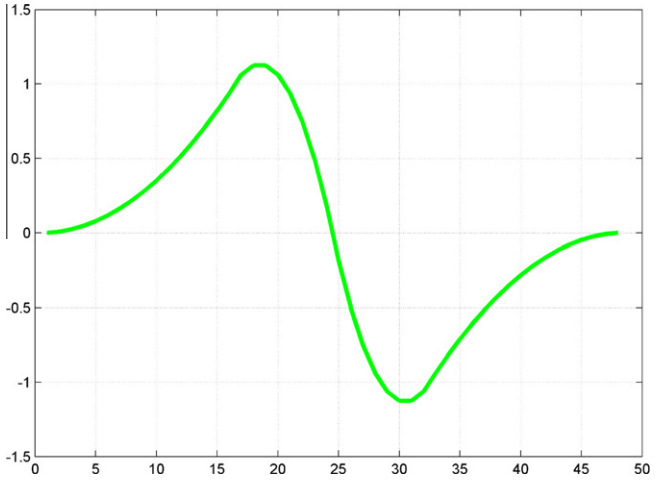

Fig. 10. The wavelet Ψ of wavelet rbio3.1.

Table 6
Decomposition filter coefficients for wavelet rbio3.1 ($h_0(k)$—lowpass, $h_1(k)$—highpass).

$h_0(k)$	0.1768	0.5303	0.5303	0.1768
$h_1(k)$	0.3536	1.0607	−1.0607	−0.3536

For the presented analysis, a maximum fifth order of the wavelet decomposition was assumed to obtain a separate feature vector for testing — see Fig. 8.

Thus, the final selection should be made from 881 different feature vectors — signature candidates, obtained using 73 wavelets; see Table 1. The results of this research were developed in two

Fig. 11. Visualization of an example binary template obtained from iris biometrics (length: 324 bits).

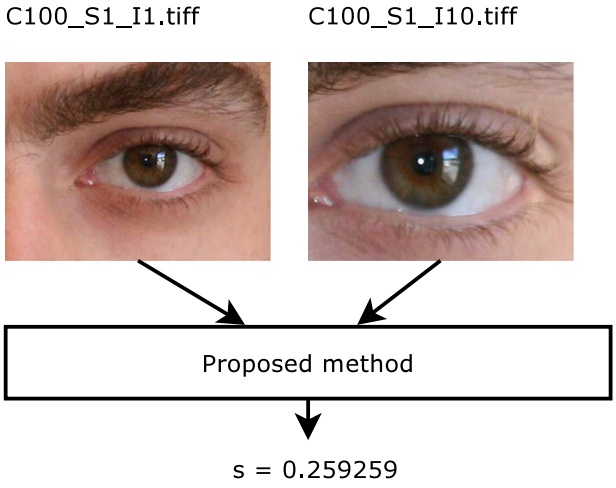

Fig. 12. An example of similarity score s for matching of irises from the same person.

Fig. 14. An example of similarity score s for matching of irises from different persons.

ways: as the Equal Error Rate (EER), the single parameter that directly characterizes authentication error tradeoff at $FAR = FRR$ operating point, and as the d′, the evaluation criterion within the NICE.II contest. The results are summarized in Tables 2–5 respectively. The analysis used 5000 comparisons of the 500,000 in the NICE.II training set for the test.

According to this analysis, it appears that the best wavelet choice for iris feature extraction using DWT is the rbio2.2 wavelet because it gives the lowest EER and the highest d′ value. However, in other authors' studies made on the basis of the UBIRISv.1 database, as presented elsewhere (Szewczyk, 2007), the rbio3.1 wavelet gave the best recognition result. Depending on the previous and the current work, this wavelet was selected for the contest as it additionally results in a highly compact output signature. Moreover, from the above results and from the research already presented in the literature, the best wavelet choice can vary significantly depending on the database and other factors; see (Moukhtar et al., 2005; Thornton et al., 2007; Minhas et al., 2009; Narote et al., 2009). Thus, there is no versatile filter type for the iris feature extraction stage.

2.4. Signatures encoding

On the basis of the conclusions from the previous section, the iris image shown in Fig. 6 was encoded using DWT and the rbio3.1 wavelet. The rbio3.1 (with the scaling function ϕ presented in Fig. 9 and the wavelet Ψ – in Fig. 10) is compactly supported by a biorthogonal spline wavelet for which symmetry is possible with FIR filters (see Table 6) and three vanishing moments (Daubechies, 1992).

To generate the signature, the V4 component is chosen from the wavelet decomposition tree, as shown in Fig. 7. This component is particularly sensitive to significant elements inside the iris structure, which increases the algorithm robustness because small changes in iris structure are rejected from the feature set. Additionally, the feature vector obtained at a 4th order of decomposition does not contain much information about the high-frequency noise, because this information is wiped out by the approximation during several decomposition stages. Because of the size of the input image, which was 256×256 pixels, the digital template estimated from the V_4 component consists of 324 coefficients, which gives compact representation.

After the wavelet image decomposition, an iris signature composed of real coefficients ($\{V4 : V4_i \in \mathbf{R}\}$) is obtained. The vector elements must be translated into binary template $\{\widehat{T} : \widehat{T}_i \in \{0,1\}\}$. This allows the use of simpler tools for template matching in the following stages. On the basis of the authors' preliminary research presented elsewhere (Szewczyk, 2007), the authors decided to use a median-based transformation:

$$\widehat{T}_i = \begin{cases} 0 & \text{if } V4_i < \text{median}(V4) \\ 1 & \text{for others} \end{cases}. \tag{7}$$

The visualization of a resulting binary template is shown in Fig. 11.

The final encoding phase reduces the size of an iris biometric representation to 324 bits of digital template. Taking into consideration the size of an input image equal to 512×256 pixels and 24 bits of radiometric resolution, the compression ratio is equal to 9709 for this solution.

2.5. Score calculation

Two binary digital templates $\widehat{T}_A$ (e.g., obtained on-line) and $\widehat{T}_B$ (e.g., stored in a database) are compared to compute the similarity score $s = s(\widehat{T}_A, \widehat{T}_B)$. The score s, together with the arbitrary chosen decision threshold t, is used for final authentication according to (8):

$$\begin{aligned} s \leqslant t &\rightarrow \text{ match} \\ s > t &\rightarrow \text{ not match} \end{aligned} \tag{8}$$

Fig. 13. Comparison of binary signatures for matching of irises from the same person (C100_S1_I1, C100_S1_I10).

Fig. 15. Comparison of binary signatures for matching of irises from different persons (C100_S1_I1, C101_S1_I1).

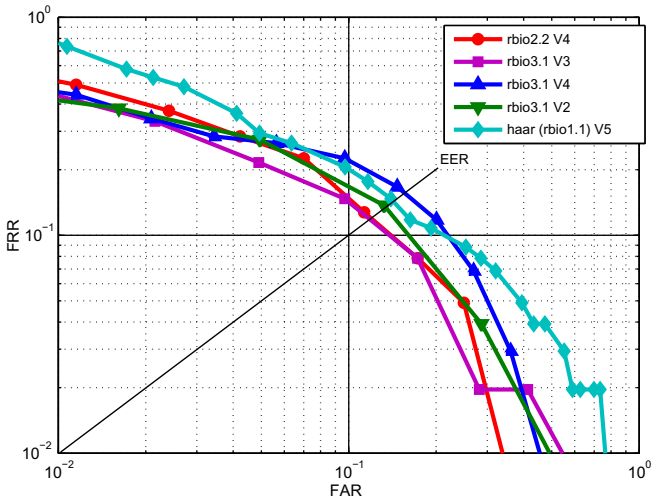

Fig. 16. The DET curves for the proposed method obtained using the UBIRISv.2 database.

As a biometric comparator, the Hamming Distance (HD) measure was chosen because it is very well-known and most widely used tool for this purpose in the field; see, for example, (Daugman, 1993; Daugman, 2004). The measure is basically obtained in two steps. In the first, the logical operation XOR of two binary vectors of length N is performed. Afterwards, the number of ones — differences between compared vectors on the particular positions — is summed. The final similarity score s is obtained by dividing the obtained sum by N, which is formally expressed in (9). The segmentation mask is not taken into account for the purpose of score calculation in the algorithm submitted for the NICE.II contest.

$$s = s(\widehat{T}_A, \widehat{T}_B) = \frac{1}{N}\sum_{i=1}^{N} \widehat{T}_A(i) \oplus \widehat{T}_B(i). \tag{9}$$

Additional advantages of this parameter are efficiency, ease of implementation and a value that is easy to interpret within statistical theory. The similarity score is somewhat similar to evidence in a zero or alternative hypothesis, according to Wayman's formalism (Wayman, 1997). For formula (8), a lower score denotes stronger evidence for the hypothesis that the compared biometric templates are from the same person; higher values of the score indicate stronger evidence that the compared templates are evaluated from different persons.

An example of the comparison of iris images that are from the same person is presented in Figs. 12 and 13, while an example of imposter comparison is presented in Figs. 14 and 15.

3. Result analysis

As a compact measure for algorithms reported to the NICE.II contest, the statistical metric d' was selected in order to determine their distinctiveness. The statistical metric d' is given by the following equation:

$$d' = \frac{|\mu_{t1} - \mu_{t2}|}{\sqrt{\frac{\sigma_{t1}^2 + \sigma_{t2}^2}{2}}}, \tag{10}$$

where μ_{t1}, μ_{t2} denote the mean values of a score distribution for zero ($t1$) and alternative ($t2$) hypothesis according to Wayman's formalism (Wayman, 1997) and σ_{t1}, σ_{t2} are standard deviations of those score distributions.

The d' parameter is easy to interpret. In general, a higher d' value denotes better discriminative power of the verified method because it indicates better separability of score distributions for both hypotheses and leads to lower authentication error rates: False Match Rate (FMR) and False Not-Match Rate (FNMR), (FAR and FRR, accordingly, for a positive biometric system). This statistical metric computed in the NICE:II contest for the proposed method is equal to $d' = 1.0931$.

However, to obtain more comprehensive characterization of the verified biometric method, the Detection Error Trade-off (DET) curve and Equal Error Rate (EER) can be used. The DET curves estimated for the proposed method tested with NICE database are presented in Fig. 16.

4. Conclusion

In this paper, an example strategy for iris recognition using degraded images acquired under unconstrained imaging conditions is presented. The proposed method appears to be somewhat insensitive to perspective changes, illumination conditions, occlusion variable grade and reflections from the eye's surface, which is especially troublesome in visible wavelength imaging.

In general, the proposed algorithm flow is common to other solutions presented in the literature. However, the main advantages of the proposed solution are a compact signature, which is 324 bits wide, increase of iris image SNR by removing the most noisy blue channel, and a procedure for distinctive noise-free area selection. Although the overall algorithm flow is simple and uses a signature shorter than commercially available solutions, for example, Daugman's signature (2048 bits), it can be successfully used for recognition of people based on iris patterns, which was shown on the basis of the FAR and FRR trade-off in Fig. 16.

References

Abhyankar, A., Schuckers, S., 2009. Iris quality assessment and bi-orthogonal wavelet based encoding for recognition. Elsevier Pattern Recog. J. 42 (9), 1878–1894.

Abhyankar, A., Schuckers, S., 2010. A novel biorthogonal wavelet network system for off-angle iris recognition. Elsevier Pattern Recog. J. 43 (3), 987–1007.

Ali, J.M.H., Hassanien, A.E., 2003. An iris recognition system to enhance e-security environment based on wavelet theory. AMO J. 5 (2), 93–104.

Boles, W.W., 1996. A wavelet transform based technique for the recognition of the human iris. Fourth Internat. Symposium on Signal Processing and Its Applications 2, 601–604.

Boles, W.W., 1997. A security system based on human iris identification using wavelet transform. First Internat. Conf. on Knowledge-Based Intelligent Electronic Systems 2, 533–541.

Boles, W.W., Boashash, B., 1998. A human identification technique using images of the iris and wavelet transform. IEEE Trans. Signal Process. 46 (4), 1185–1998.

Bolle, R.M., Connel, J.H., Pankanti, S., Ratha, N.K., Senior, A.W., 2004. Guide to Biometrics. Springer Science & Buisness Media Inc., New York.

Daouk, C.H., Esber, L., Kanmoun, F.O., Alaoui, M.A., 2002. Iris recognition, Proc. ISSPIT, 558–562.

Daubechies, I., 1992. Ten lectures on wavelets, CBMS-NSF Lecture Notes, No. 61, SIAM.

Daugman, J., 1993. High confidence visual recognition of persons by a test of statistical independence. IEEE Trans. Pattern Anal. Machine Intell. 15 (11), 1148–1161.

Daugman, J., 1994. Biometric personal identification system based on iris analysis, US Patent 5, 291, 560.

Daugman, J., 2004. How iris recognition works. Trans. Circ. Syst. Video Technol. 14, 21–30.
Daugman, J., 2007. New methods in iris recognition. IEEE Trans. Systems Man Cybernet. Part B 37 (5), 1167–1175.
Kim, D.H., Ryoo, J.S., 2001. Iris identification system and method of identifying a person through iris recognition, US Patent 6,247,813 B1.
Kim, J., Cho, S., Choi, J., Marks, R.J., 2004. Iris recognition using wavelet features. J. VLSI Signal Process. 38 (2), 147–156.
Kumar, A., Passi, A., 2008. Comparison and combination of iris matchers for reliable personal identification, Proc. Computer Society Conf. on Computer Vision and Pattern Recognition Workshops, pp. 1–7.
Lim, S., Lee, K., Byeon, O., Kim, T., 2001. Efficient iris recognition through improvement of feature vector and classifier. ETRI J. 23 (2), 61–70.
Ma, L., Tan, T., Wang, Y., Zhang, D., 2003. Personal identification based on iris texture analysis. IEEE Trans. Pattern Anal. Machine Intell. 25 (12), 1519–1533.
Ma, L., Tan, T., Wang, Y., Zhang, D., 2004. Efficient iris recognition by characterizing key local variations. IEEE Trans. Image Process. 13 (6), 739–750.
Matey, J., Naroditsky, O., Hanna, K., Kolczynski, R., Lolacono, D., Mangru, S., Tinker, M., Zappia, T., Zhao, W., 2006. Iris on the move: Acquisition of images for iris recognition in less constrained environments, Proceedings of the IEEE, Vol. 94, No. 11, pp. 1936 –1947.
Minhas, S., Javed, M., Basit, A., 2009. Iris feature extraction using wavelet transform, Proc. IASTED Internat. Conf., Signal and Image Processing, pp. 198–203.
Moukhtar, E., El-Kadi, M., Hazem, M., Bakhoum, M., Bahgat, R., Mossaad, R., El-Sherief, S.A.S., ElDin, S.N., Fakhr, W., 2005. Rejection analysis of an iris recognition system, Proc. Internat. Cong. on GVIP.
Narote, S., Narote, A., Waghmare, L., 2009. Iris based recognition system using wavelet transform. IJCSNS Internat. J. Comput. Sci. Network Secur. 9 (11), 101–104.
Noh, Seung-In, Bae, K., Park, Y., Kim, J., 2003. A Novel Method to Extract Features for Iris Recognition System. In: Kittler, J., Nixon, M. (Eds.), Audio- and Video-Based Biometric Person Authentication, Ser. Lecture Notes Comput. Sci., vol. 2688. Springer, Berlin/ Heidelberg, p. 1054.
Poursaberi, A., Araabi, B., 2005. A novel iris recognition system using morphological edge detector and wavelet phase features. GVIP J. 6, 9–15.
Proenca, H., Alexandre, L.A., 2010. Image and Vision Computing, Special Issue On the Segmentation of Visible Wavelength Iris Images Acquired At-a-Distance and On-the-Move, vol. 28, No. 2, Elsevier.
Proenca, H., Filipe, S., Santos, R., Oliveira, J., Alexandre, L.A., 2010. The UBIRIS.v2: A database of visible wavelength iris images captured on-the-move and at-a-distance. IEEE Trans. Pattern Anal. Machine Intell. 32 (8), 1529–1535.
Sankowski, W., 2009. Eye image segmentation algorithms for an iris identification system based on an iris pattern, Ph.D. thesis, Technical University of Lodz, Department of Microelectronics and Computer Science.
Sankowski, W., Grabowski, K., Zubert, M., Napieralska, M., 2010. Reliable algorithm for iris segmentation in eye image. Elsevier Image Vision Comput. J. 28, 231–237.
Seong-Won, C., 2002. Method of recognizing human iris using wavelet transform, Republic of Korea Patent WO02 071 317 A1.
Strang, G., Nguyen, T., 1996. Wavelets and Filter Banks, Wellesley-Cambridge Press, Preface, page xiv.
Sun, Z., Tan, T., Qiu, X., 2005. Graph Matching Iris Image Blocks with Local Binary Pattern. In: Zhang, D., Jain, A. (Eds.), Advances in Biometrics, Ser. Lecture Notes Comput. Sci., vol. 3832. Springer, Berlin/ Heidelberg, pp. 366–372.
Sung, H., Lim, J., Park, J.-h., Lee, Y., 2004. Iris recognition using collarette boundary localization, Proc. 17th Internat. Conf. on Pattern Recognition 4, 857–860.
Szewczyk, R., 2007. New features extraction method for people recognition on the basis of the iris pattern, 14th Internat. Conf. on Mixed Design of Integrated Circuits and Systems, pp. 645–650.
Thornton, J., Savvides, M., Kumar, B.V., 2007. An evaluation of iris pattern representations, Proc. First IEEE Internat. Conf. on Biometrics: Theory, Applications, and Systems, pp. 1–6.
Wayman, J., 1997. A scientific approach to evaluating biometric systems using mathematical methodology, Proc. CardTech SecureTech Conf., pp. 477–492.
Wildes, R.P., 1997. Iris recognition: an emerging biometric technology. Proc. IEEE 85(9), 1348–1363.